

## Evidence of surface transport and weak antilocalization in a single crystal of the $\text{Bi}_2\text{Te}_2\text{Se}$ topological insulator

Chandra Shekhar,<sup>\*</sup> C. E. ViolBarbosa, Binghai Yan, Siham Ouardi, W. Schnelle, Gerhard H. Fecher, and Claudia Felser<sup>†</sup>  
*Max Planck Institute for Chemical Physics of Solids, 01187 Dresden, Germany*

(Received 9 June 2014; revised manuscript received 7 October 2014; published 30 October 2014)

Topological insulators are known for their metallic surface states, a result of strong spin-orbit coupling, that exhibit unique surface transport phenomenon. However, these surface transport phenomena are buried in the presence of metallic bulk conduction. We synthesized very high quality  $\text{Bi}_2\text{Te}_2\text{Se}$  single crystals by using a modified Bridgman method that possess high bulk resistivity of  $>20 \Omega\text{cm}$  below 20 K, whereas the bulk is mostly inactive and surface transport dominates. The temperature dependence of resistivity follows an activation law like a gap semiconductor in temperature range 20–300 K. To extract the surface transport from that of the bulk, we designed a special measurement geometry to measure the resistance and found that single-crystal  $\text{Bi}_2\text{Te}_2\text{Se}$  exhibits a crossover from bulk to surface conduction at 20 K. Simultaneously, the material also shows strong evidence of weak antilocalization in magnetotransport owing to the protection against scattering by conducting surface states. This simple geometry facilitates finding evidence of surface transport in topological insulators, which are promising materials for future spintronic applications.

DOI: [10.1103/PhysRevB.90.165140](https://doi.org/10.1103/PhysRevB.90.165140)

PACS number(s): 72.20.Fr, 72.15.Gd, 73.20.At, 73.25.+i

### I. INTRODUCTION

Topological insulators (TIs) have recently attracted significant attention since they have been shown to be a new state of quantum matter and they possess topologically protected metallic states on their edges or surfaces [1,2]. These conducting surface states (SSs) originate from the inversion of bulk bands as a result of strong spin-orbit coupling. Therefore, these novel metallic states are a subject of intensive investigations because of not only their fundamental novelty but also their potential applications for spintronics devices [3] and quantum computations [4].

In three-dimensional (3D) TIs, topological surface states have been successfully investigated by surface-sensitive techniques such as angle-resolved photoemission spectroscopy [5,6] and scanning tunneling microscopy [7,8]. Besides these extensive observations, optical spectroscopy is another experimental tool that shows the evidence of metallic surface, and a coherent surface state transport has been found in optical conductivity [9–13]. However, finding evidence of transport through the surface states remains a challenge owing to the presence of parallel bulk conducting channels that usually dominate the transport properties [14–16]. Various strategies to improve surface conductivity (e.g., by studying thin films or nanoflakes [6,17–21], gating [20,22,23], and doping [15,16,24]) have been employed. Among the known TIs, the ternary *tetradymite*  $\text{Bi}_2\text{Te}_2\text{Se}$  (BTS) has been a widely investigated material because it gives excellent surface performance with temperature-dependent resistivity [6,17–21,25]. It exhibits large bulk resistivity owing to its nearly perfect crystalline structure, and it has been predicted to be nearly perfect Dirac cones in terms of less entanglement of bulk and surface states [6,21,24,25]. Quantum oscillations have also been observed in BTS [25–27] and doped BTS [15,24] bulk samples, and these observations show that

surfaced-dominated transport contributes up to 70% of the total conductance [15,25]. In addition to this metallic behavior, excellent performance of the surface states of TIs appears in magnetoconductance via weak antilocalization (WAL), which is observed in thin films or nanoflakes only [6,21]. In view of these promising advances, exploration of the topologically protected surface transport in bulk TIs appears to be achievable. Very recently,  $\text{SbB}_6$  has been identified as a topological insulator [28,29], it exhibits surface-dominated transport below 4 K in resistivity, which has been measured in the specialized geometry of single crystals [30,31].

The main goal of the present work is to explore the performance of the BTS compound as a TI in state-of-the-art high-quality crystals. The resistance of our BST crystal exhibits a steep growth with decreasing temperature and starts to saturate at  $T \leq 30$  K. This steep growth appears in the form of activation energy with  $\Delta = 28.1$  meV in the temperature range of 300–30 K; below 30 K it exhibits metallic character owing to the presence of topological SSs, which is the main attraction of a TI. We explored these surface states by measuring resistance in a specially designed geometry and our results show a crossover from bulk to surface conduction below 20 K. Besides this, the magnetoconductance provides clear evidence of WAL, which also indicates a strong contribution of topological SSs.

### II. EXPERIMENTAL DETAILS

Single crystals of BTS were grown from high-purity (99.999%) bismuth (Bi), tellurium (Te), and selenium (Se) chips and ingots by using a modified Bridgman method. First, the elements were loaded in the proper stoichiometric ratio into a dry alumina tube and then put into a dry quartz tube. The tube was evacuated ( $10^{-6}$  torr) and sealed. The sealed ampoule was loaded into the vertical Bridgman furnace and heated slowly to form a single phase. The ampoule was heated to  $800^\circ\text{C}$  at  $60^\circ\text{C/h}$  and then kept at this temperature for 12 h. For single-crystal growth, the temperature was slowly reduced

<sup>\*</sup>shekhar@cpfs.mpg.de

<sup>†</sup>felser@cpfs.mpg.de

by 2 °C/h from 800 to 500 °C and the ampoule was annealed for a week at 500 °C before being cooled to room temperature. This procedure resulted in silver-colored single crystals of 10 mm in size. The slow cooling rate and extra annealing procedures were followed to minimize defects in the form of Se vacancies, which are invariably found in Se containing *tetradymite* compounds. The crystals were confirmed to be single phase and identified as having rhombohedral  $\text{Bi}_2\text{Te}_2\text{Se}$  crystal structure by x-ray diffraction. X-ray diffraction patterns (not shown here) of the cleaved crystals oriented with the basal plane normal bisecting the incident and diffracted beam directions showed only the (006), (009), and (0012) peaks (hexagonal setting), indicating that the cleaved surface is oriented perpendicular to the hexagonal  $c$  axis. The x-ray results revealed a hexagonal structure with space group  $R\bar{3}m$  (No. 166). The lattice parameters were determined to be  $a = 4.283 \text{ \AA}$  and  $c = 29.667 \text{ \AA}$ . The observed values are in good agreement with those reported previously [22,32].

### III. RESULTS AND DISCUSSION

To explore the transport properties, we performed the usual four-probe method to measure normal resistance and five-probe Hall resistance of bulk BTS single crystals of dimensions  $2.6 \times 0.4 \times 5.2$  ( $w \times d \times l$ )  $\text{mm}^3$  in the temperature range of 2–300 K and with magnetic fields of up to 9 T. Ohmic contacts were made by using a conductive silver epoxy. Figure 1 shows the temperature dependency of the electrical resistance  $R(T)$  and Hall coefficient  $R_H(T)$ . The overall zero-field temperature dependency of the resistance is shown in Fig. 1(a). The magnitudes of  $R(T)$  are 1  $\text{k}\Omega$  at 2 K and 0.2  $\Omega$  at 290 K, indicating that a change of more than three orders of magnitude in resistance is found and that resistance steeply increases with temperature from 300 to 30 K, reflecting that the sample possesses a band gap. This saturation temperature is similar to that previously observed in the BTS compound [6,18,20,21,25–27]. After saturation, the resistance reaches its maximum point at 20 K and then start to decreases. A fitted blue line in Fig. 1(c) shows the metallic behavior below 20 K owing to the presence of metallic SSs of TIs, which are the main attraction of TIs. To gain a broader insight into the charge transport mechanism, we carefully analyzed the variation of resistance in the high-temperature range by plotting  $\ln(1/R)$  versus  $(1/T)$  as shown in Fig. 1(c). The  $\ln(1/R)$  data from 300 to 40 K is very well fitted by an activated transport model with  $\Delta = 28.1 \text{ meV}$ . This transport behavior and value of  $\Delta$  are similar to those of other reported BST crystals [24,27]. This indicates that the large bulk resistivity of this compound can be achieved by taking a stoichiometric ratio of initial elements, thereby avoiding having to manipulate the initial elemental ratios [15,16,24,27]. Here an important point is that the rather low crossover temperature in resistivity shows surprisingly high resistance and large activation energy, which can be understood in term of suppression of the surface state transport due to bulk phonon mediated transport [9].

Figure 1(b) summarizes the result obtained from Hall measurements. The Hall coefficient changes sign from positive to negative as temperature is changed from high to low. This result is similar to those of other reports [6,26,27], where negative charge carriers dominate at low temperatures. The

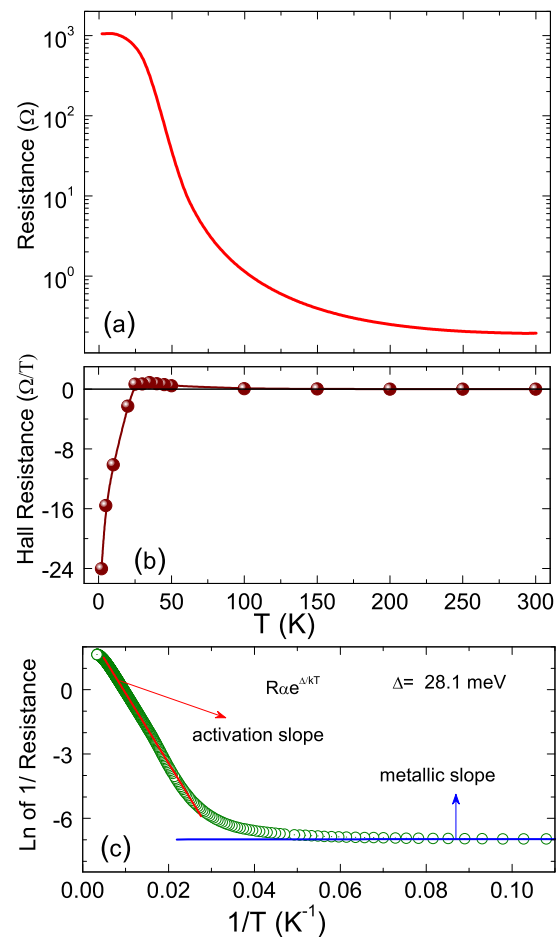


FIG. 1. (Color online) Temperature dependence of (a) four-probe resistance of the bulk single crystal and (b) five-probe Hall coefficients. (c) Plot of  $\ln(1/R)$  vs  $(1/T)$ ; the resistance follows the Arrhenius law  $R = R_0 e^{-\Delta/kT}$  in the temperature range between 300 and 30 K as indicated by the straight red line; after that it follows metallic behavior (blue line).

large change in resistance is related to its intrinsic behavior; however, the high value of the Hall coefficient, i.e., low carrier density, is related to the presence of minimum defects in the sample. Most of the reduction in  $R(T)$  with increasing temperature is mainly due to an increase of the carrier concentration, except below 20 K, where the concentration of charge carriers saturates.

The main attraction of TIs is the transport through SSs, but this is usually buried in the presence of bulk conduction. The plotted resistance in Fig. 1(a), measured by using a conventional four-probe method, shows a temperature dependence behavior that is similar to that previously reported. At temperature  $>30 \text{ K}$ , a uniform current passes through the whole material owing to bulk conduction but these currents are forced to flow through only the surface when the bulk becomes insulating at temperature  $<30 \text{ K}$ , where the compound exhibits metallic behavior. To extract the surface transport from the bulk of a well-characterized crystal, we measured the four-probe resistance in a special geometry, putting the voltage and current contacts at unusual positions [30]. Here  $V_{\text{lat}}$  is the normal voltage, which has been measured in such a way that the

voltage and current contacts lie on the same surface (front surface), and  $V_{\text{hyb}}$  is the bulk voltage, which has been measured by putting the current and voltage contacts on opposite surfaces (current contacts on the front surface and voltage contacts on the back surface). However,  $V_{\text{vert}}$  is a voltage that has been measured by putting one voltage and one current contact on the same surface (front surface) but the other two contacts on the opposite surface (back surface). This  $V_{\text{vert}}$  value is measurable only when the surface is conducting; otherwise, this is not measurable owing to the conducting bulk. To avoid the flow of current in other directions, we made the contacts after half of the sample length, whereas all the voltage contacts lie on their own respective path of the majority current. Such typical contact configurations are illustrated in Fig. 2, and measured resistances according to these configurations are shown in Fig. 3. If the material is a bulk conductor, the current paths shown in Figs. 2(a) and 2(c) will be the major paths; otherwise, current will follow the paths depicted in Figs. 2(b) and 2(d), which are for the case of surface transport. Therefore, the measured resistances  $R_{\text{lat}}$ ,  $R_{\text{hyb}}$ , and  $R_{\text{vert}}$  are extremely different from each other and their values depend upon their

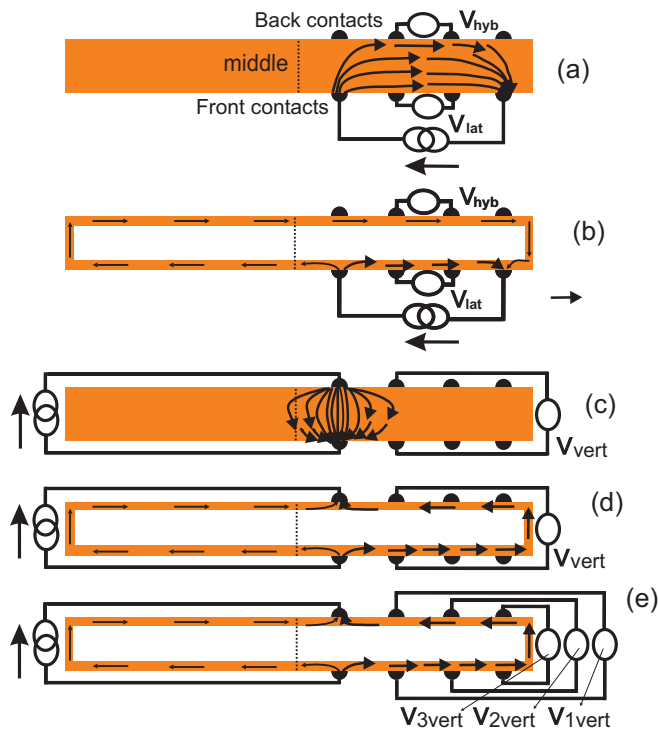


FIG. 2. (Color online) Horizontal cross sections of the sample along with eight coplanar electrical contacts, four on each side. (a) The current goes laterally through the bulk, and the front-side and back-side voltages give the same values. (b) The bulk in (a) becomes insulating, the current is forced to flow along the edge (i.e., along the surface in the sample), and front voltage contacts become isolated from back contacts. (c) The current flows horizontally through the bulk and voltage contacts are far away from the major current path. (d) The bulk in (c) becomes insulating, and the current is forced to flow along the edge. (e) Measurement of the voltage in (d) at three consecutive contacts. All these diagrams have been constructed by assuming isotropic transport; thick and thin arrows indicate the major and minor current directions, respectively.

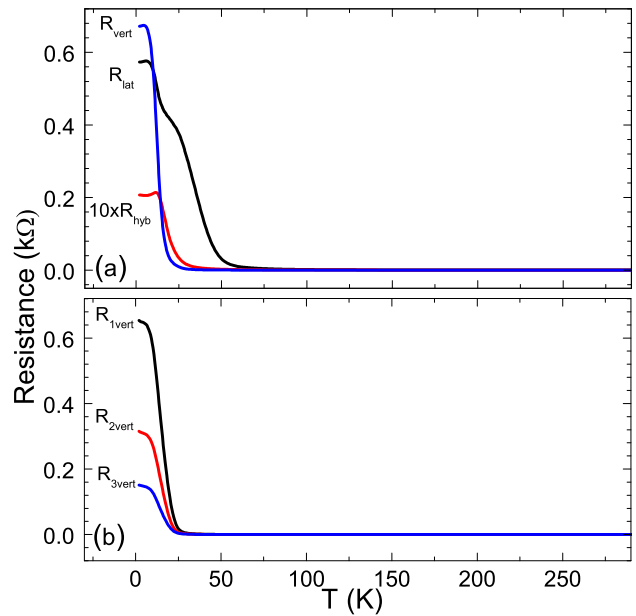


FIG. 3. (Color online) Temperature dependence of resistances measured in a special configuration: (a)  $R_{\text{lat}}$ ,  $R_{\text{hyb}}$ , and  $R_{\text{vert}}$ ; (b)  $R_{\text{vert}}$  at three consecutive points in the same configuration.

current paths. In the case of bulk conduction,  $R_{\text{lat}}$  and  $R_{\text{hyb}}$  should be equal because the same amount of current passes between  $V_{\text{lat}}$  and  $V_{\text{hyb}}$  probes but  $R_{\text{vert}}$  is very low because only a negligible amount of current flows between  $V_{\text{vert}}$  probes. The resistance magnitudes found follow  $R_{\text{lat}} > R_{\text{hyb}} > R_{\text{vert}}$ , as would be expected for bulk conduction at high temperature. However, for surface conduction or the TI case below 30 K, where current is forced to flow through the surface,  $R_{\text{lat}}$  becomes larger than  $R_{\text{hyb}}$  because  $V_{\text{lat}}$  and  $V_{\text{hyb}}$  probes lie on the major current path on the front surface and on the minor current path on the back surface, respectively. However,  $R_{\text{vert}}$  is highest because the  $V_{\text{vert}}$  contacts lie on the majority current path, which is also longer than the path of the  $V_{\text{lat}}$  probes [30]. The measured data are shown in Fig. 3 and are consistent with surface and bulk transport. To explore the resistance  $R_{\text{vert}}$  further, we measured it at three consecutive points as shown in Fig. 2(e). The measured resistances  $R_{1\text{vert}}$ ,  $R_{2\text{vert}}$ , and  $R_{3\text{vert}}$  are displayed in Fig. 3(b). Here  $R_{1\text{vert}}$  is highest and  $R_{3\text{vert}}$  is lowest; again, this is consistent with their current paths:  $R_{1\text{vert}}$  covers the longest path but  $R_{3\text{vert}}$  covers the shortest path according to surface transport.

To obtain better insight into transport properties in the low-temperature range, we investigated the magnetoconductance in a tilted field. For this purpose we chose a temperature range in the metallic region, which has already been explained in Figs. 1 and 3. The nature and values of the magnetoconductance strongly depend on the applied fields, as shown in Fig. 4.  $\Delta G_{2D}$  represents the change of the two-dimensional (2D) conductance ( $G_{2D}$ ) with the field and is estimated as  $G_{2D} = G(d/w)$ , where  $G = 1/R$  and  $d$  is the distance between voltage probes. The symbols in Fig. 4(a) represent the experimental data. The sharp increase of the conductivity at low fields, forming a steep cusp, is a well-known signature of WAL. The WAL effect arises in a phase-coherent

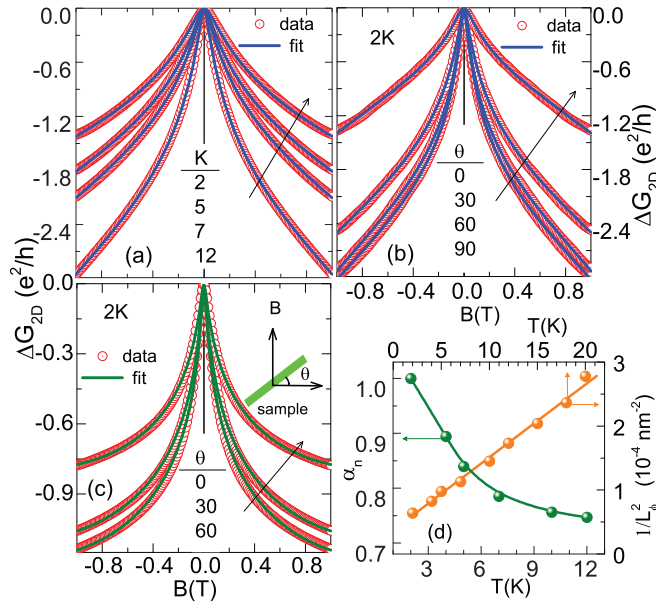


FIG. 4. (Color online) (a) Temperature dependence of conductivity at  $\theta = 0^\circ$ . (b) Conductivity measured in tilted  $B$  fields, where the blue line is a fitting by the Hikami-Larkin-Nagaoka (HLN) 2D model of Eq. (2). (c) Perfect 2D data in tilted  $B$  fields, obtained by subtracting tilted data with  $\theta = 90^\circ$ , where the green line is a fitting by only the first term of the HLN 2D model of Eq. (2). (d) Temperature dependence of normalized  $\alpha_n = \alpha/\alpha_{2K}$  (left axis) and  $1/L_\phi^2$  (right axis). Inset of (c) shows sample rotation geometry with field.

conductor when destructive interference occurs between two time-reversed electron paths. This destructive interference inhibits elastic backscattering, thereby increasing the conductivity.

This WAL effect is found only in thin films or nanoflakes of TIs [6,21,33] and originates from strong spin-orbit coupling in the bulk, resulting in spin-momentum locking in the topological SSs [34]. The response of the conductance to the magnetic field in a 2D system with WAL can be quantified by using a well-known Hikami-Larkin-Nagaoka (HLN) model [35]:

$$\begin{aligned}
 \Delta G_{2D}^{\text{HLN}} &= G_{2D}(B) - G_{2D}(0) \\
 &= \alpha \frac{e^2}{2\pi h} \left[ \Psi \left( \frac{1}{2} + \frac{B_\phi}{B} \right) - \ln \left( \frac{B_\phi}{B} \right) \right] \\
 &\quad + \alpha \frac{e^2}{\pi h} \left[ \Psi \left( \frac{1}{2} + \frac{B_{\text{so}} + B_e}{B} \right) - \ln \left( \frac{B_{\text{so}} + B_e}{B} \right) \right] \\
 &\quad + \alpha \frac{3e^2}{2\pi h} \left[ \Psi \left( \frac{1}{2} + \frac{(4/3)B_{\text{so}} + B_e}{B} \right) - \ln \left( \frac{(4/3)B_{\text{so}} + B_e}{B} \right) \right], \quad (1)
 \end{aligned}$$

where  $B_i$  are the characteristic fields of each respective scattering channel ( $i = \phi, \text{so}, e$ ) given by  $B_i = \hbar/(4eL_i^2)$ ,  $\Psi$  is the digamma function,  $L_\phi$  is the phase coherence length (traveled length without coherency break),  $L_{\text{so}}$  is the spin-orbit scattering length, and  $L_e$  is the elastic scattering

length (or the mean free path). At low temperatures and small fields, the coherence length is the longest among these three lengths; therefore, phase coherence scattering dominates over existing scattering [19]. At high fields, the  $L_{\text{so}}$  and  $L_e$  lengths become prominent and yield characteristic fields of the order of several tesla. The latter two terms containing spin-orbit scattering and elastic scattering can easily be approximated into a  $B^2$  term. Therefore, this approximation leads to

$$\Delta G_{2D} = \alpha \frac{e^2}{2\pi h} \left[ \Psi \left( \frac{1}{2} + \frac{B_\phi}{B} \right) - \ln \left( \frac{B_\phi}{B} \right) \right] - cB^2. \quad (2)$$

This has already been applied earlier [19]. Here  $\alpha$  indicates the type of localization and is equal to  $-1$  for WAL in a perfect 2D system. In our case, the fitted values of  $\alpha$  are 3.1–2.3 in the temperature range of 2–20 K. We considered that the highest conduction through the surface states occurs at 2 K and took the value of  $\alpha$  at 2 K as a reference. The normalized values  $\alpha_n$  ( $\alpha/\alpha_{2K}$ ) range from 1.0 to 0.75 between 2 and 12 K, as shown in Fig. 4(d). These values decrease with increasing temperature and reveal that the surface contributions decrease with increasing temperature. The other fitting parameter is  $L_\phi$ , which is directly related to  $B_\phi$ . The 2D nature of conductivity exhibits a more qualitative temperature dependence of  $L_\phi$  that varies with  $T^{-0.5}$  for inelastic electron-electron interactions [36,37]. From Fig. 4(d), the temperature dependence of  $1/L_\phi^2$  exhibits a linear behavior, indicating the dominant inelastic electron-electron scattering in the surface conducting channels of our BST bulk single crystal [6,18–20]. The depth and magnitude of the conductivity also decrease as temperature increases [see Fig. 4(a)] because of the decrease of  $L_\phi$ . The WAL is also seen up to 147 K [19]. The main outcome of the HLN fit is the values of  $\alpha$  and  $L_\phi$ , which relate the number of active conducting channels and distance traveled by charge carriers before dephasing, respectively. For WAL of any TI, the value of  $\alpha$  is experimentally found to be  $\sim -0.5$  per conducting channel, but there is no theoretically predicted value of  $\alpha$  [6,18–20]. To clarify the perfect 2D WAL effect in our bulk sample, the conductivity measured in tilted magnetic fields at 2 K is shown in Fig 4(b). At  $\theta = 90^\circ$ , i.e.,  $B$  in sample plane along the current direction, the conductivity dip feature still appears. If the conduction is only through SSs, this dip in conductivity vanishes at  $\theta = 90^\circ$ , but this is not the case here [38]. For better understanding, the conductance at  $\theta = 90^\circ$  is named as bulk conductance, i.e., 3D conductance that origin is not yet clear [20,38]. But it might have originated from the conduction of those electrons, which do not move along the current direction, i.e., conduct along side wall surfaces and mesas of the top and bottom surfaces of the crystal. To obtain only the 2D conductivity, the 3D conductivity at  $\theta = 90^\circ$  was subtracted from the measured conductivity at another angle. The resultant data are plotted and fitted by HLN theory with only the first term in Fig. 4(c). This fit yields  $\alpha = 1.02$  and  $L_\phi = 212$  nm at  $\theta = 0^\circ$ , which are perfectly matched with results from other reports and indicate the 2D transport through SSs [20,38].

The observed values of  $\alpha$  in the literature cover a wide range from  $-0.4$  to  $-2.5$ , suggesting that it depends on (i) sample thickness [19,39], (ii) the presence of bulk conductivity gating

[20,22,23], and (iii) the substrate [38]. Thin films of TIs, which are prepared on the substrate through a different route, have an  $\alpha$  value of  $\sim 0.5$  [23,38,40]. However, the value of  $\alpha$  also depends on the number of conduction channels, and  $\alpha$  can even become  $-1$  when both the top and the bottom surfaces of a crystals or films contribute independently [18,41]. Values of  $\alpha$  have also been tuned between 0.5 and 1.0 by applying gate voltage [23,42]. Kim *et al.* have observed WAL in a wide range of thicknesses from 3.0 nm to 0.17 mm on Bi<sub>2</sub>Se<sub>3</sub> films, where values of  $\alpha$  exhibit increasing trend with thickness [39]. Such higher values can be explained by assuming conduction through multiple channels, i.e., some bulk channels conduct together with SSs of TIs [43]. This is a plausible reason for the higher values of  $\alpha$  in our BTS single crystal. It should also be noted here that the values of  $L_\phi$  from the literature are usually larger than the film thickness and this makes the whole sample effectively more two dimensional [38,40], i.e., the sample itself, including the bulk and SSs, acts as a 2D transport system. The surface states cannot completely contributed to this type of 2D transport behavior. Our fitted  $L_\phi$  varies from 125 to 60 nm in the temperature range of 2–20 K; these values are much smaller than the thickness (0.4 mm) of the sample and indicate greater two dimensionality. Therefore, the unusually measured resistance and strong WAL effects provide strong evidence of surface transport in BTS crystal.

#### IV. CONCLUSION

In summary, we found evidence of surface transport in a highly bulk resistive single-crystal Bi<sub>2</sub>Te<sub>2</sub>Se topological insulator. At temperature  $< 30$  K, the resistivity exhibits metallic behavior owing to the presence of conducting surface states. The resistance measured in special geometry differentiates the transport between bulk and surface. The magnetoconductance gives evidence of a weak antilocalization effect, which is mainly contributed by 2D surface states. The measured resistances with and without a magnetic field together indicate that surface transport dominates over bulk transport below 30 K. Therefore, this material opens up new opportunities for further physical investigations and offers a wide range of applications for topological insulators. Nonetheless, surface transport still poses a challenge at room temperature where bulk transport dominates.

#### ACKNOWLEDGMENTS

Financial support by the Deutsche Forschungsgemeinschaft (DfG, German Research Foundation) within the priority program SPP1666 “Topological insulators.” is gratefully acknowledged. B.Y. acknowledges the support of the Max-Planck-Institut für Physik komplexer Systeme in Dresden, Germany.

- 
- [1] M. Z. Hasan and C. L. Kane, *Rev. Mod. Phys.* **82**, 3045 (2010).
  - [2] X.-L. Qi and S.-C. Zhang, *Rev. Mod. Phys.* **83**, 1057 (2011).
  - [3] M. König, S. Wiedmann, C. Brüne, A. Roth, H. Buhmann, L. W. Molenkamp, X.-L. Qi, and S.-C. Zhang, *Science* **318**, 766 (2007).
  - [4] C. L. Kane, E. J. Mele, and S.-C. Zhang, *Science* **314**, 1692 (2006).
  - [5] M. Neupane, S.-Y. Xu, L. A. Wray, A. Petersen, R. Shankar, N. Alidoust, C. Liu, A. Fedorov, H. Ji, J. M. Allred, Y. S. Hor, T.-R. Chang, H.-T. Jeng, H. Lin, A. Bansil, R. J. Cava, and M. Z. Hasan, *Phys. Rev. B* **85**, 235406 (2012).
  - [6] L. Bao, L. He, N. Meyer, X. Kou, P. Zhang, Z.-g. Chen, A. V. Fedorov, J. Zou, T. M. Riedemann, T. A. Lograsso, K. L. Wang, G. Tuttle, and F. Xiu, *Sci. Rep.* **2**, 726 (2012).
  - [7] Z. Alpichshev, J. G. Analytis, J.-H. Chu, I. R. Fisher, Y. L. Chen, Z. X. Shen, A. Fang, and A. Kapitulnik, *Phys. Rev. Lett.* **104**, 016401 (2010).
  - [8] T. Zhang, P. Cheng, X. Chen, J.-F. Jia, X. Ma, K. He, L. Wang, H. Zhang, X. Dai, Z. Fang, X. Xie, and Q.-K. Xue, *Phys. Rev. Lett.* **103**, 266803 (2009).
  - [9] A. A. Reijnders, Y. Tian, L. J. Sandilands, G. Pohl, I. D. Kivlichan, S. Y. F. Zhao, S. Jia, M. E. Charles, R. J. Cava, N. Alidoust, S. Xu, M. Neupane, M. Z. Hasan, X. Wang, S. W. Cheong, and K. S. Burch, *Phys. Rev. B* **89**, 075138 (2014).
  - [10] P. Di Pietro, F. M. Vitucci, D. Nicoletti, L. Baldassarre, P. Calvani, R. Cava, Y. S. Hor, U. Schade, and S. Lupi, *Phys. Rev. B* **86**, 045439 (2012).
  - [11] A. Akrap, M. Tran, A. Ubaldini, J. Teyssier, E. Giannini, D. van der Marel, P. Lerch, and C. C. Homes, *Phys. Rev. B* **86**, 235207 (2012).
  - [12] R. Valdes Aguilar, A. V. Stier, W. Liu, L. S. Bilbro, D. K. George, N. Bansal, L. Wu, J. Cerne, A. G. Markelz, S. Oh, and N. P. Armitage, *Phys. Rev. Lett.* **108**, 087403 (2012).
  - [13] L. Wu, M. Brahlek, R. V. Aguilar, A. V. Stier, C. M. Morris, Y. Lubashevsky, L. S. Bilbro, N. Bansa, S. Oh, and N. P. Armitage, *Nat. Phys.* **9**, 410 (2013).
  - [14] N. P. Butch, K. Kirshenbaum, P. Syers, A. B. Sushkov, G. S. Jenkins, H. D. Drew, and J. Paglione, *Phys. Rev. B* **81**, 241301 (2010).
  - [15] A. A. Taskin, Z. Ren, S. Sasaki, K. Segawa, and Y. Ando, *Phys. Rev. Lett.* **107**, 016801 (2011).
  - [16] Z. Ren, A. A. Taskin, S. Sasaki, K. Segawa, and Y. Ando, *Phys. Rev. B* **84**, 075316 (2011).
  - [17] Y.-S. Fu, T. Hanaguri, S. Yamamoto, K. Igarashi, H. Takagi, and T. Sasagawa, *ACS Nano* **7**, 4105 (2013).
  - [18] B. Xia, P. Ren, A. Sulaev, P. Liu, S.-Q. Shen, and L. Wang, *Phys. Rev. B* **87**, 085442 (2013).
  - [19] B. A. Assaf, T. Cardinal, P. Wei, F. Katmis, J. S. Moodera, and D. Heiman, *Appl. Phys. Lett.* **102**, 012102 (2013).
  - [20] J. Lee, J. Park, J.-H. Lee, J. S. Kim, and H.-J. Lee, *Phys. Rev. B* **86**, 245321 (2012).
  - [21] Z. Li, T. Chen, H. Pan, F. Song, B. Wang, J. Han, Y. Qin, X. Wang, R. Zhang, J. Wan, D. Xing, and G. Wang, *Sci. Rep.* **2**, 595 (2012).
  - [22] J. Chang, L. F. Register, S. K. Banerjee, and B. Sahu, *Phys. Rev. B* **83**, 235108 (2011).
  - [23] J. Chen, H. J. Qin, F. Yang, J. Liu, T. Guan, F. M. Qu, G. H. Zhang, J. R. Shi, X. C. Xie, C. L. Yang, K. H. Wu, Y. Q. Li, and L. Lu, *Phys. Rev. Lett.* **105**, 176602 (2010).
  - [24] Z. Ren, A. A. Taskin, S. Sasaki, K. Segawa, and Y. Ando, *Phys. Rev. B* **85**, 155301 (2012).

- [25] J. Xiong, A. C. Petersen, D. Qu, R. J. Hor, Y. S. Cava, and N. P. Ong, *Physica E* **44**, 917 (2012).
- [26] S. Jia, H. Ji, E. Climent-Pascual, M. K. Fuccillo, M. E. Charles, J. Xiong, N. P. Ong, and R. J. Cava, *Phys. Rev. B* **84**, 235206 (2011).
- [27] Z. Ren, A. A. Taskin, S. Sasaki, K. Segawa, and Y. Ando, *Phys. Rev. B* **82**, 241306 (2010).
- [28] Z.-H. Zhu, A. Nicolaou, G. Levy, N. P. Butch, P. Syers, X. F. Wang, J. Paglione, G. A. Sawatzky, I. S. Elfimov, and A. Damascelli, *Phys. Rev. Lett.* **111**, 216402 (2013).
- [29] N. Xu, X. Shi, P. K. Biswas, C. E. Matt, R. S. Dhaka, Y. Huang, N. C. Plumb, M. Radovic, J. H. Dil, E. Pomjakushina, K. Conder, A. Amato, Z. Salman, D. M. Paul, J. Mesot, H. Ding, and M. Shi, *Phys. Rev. B* **88**, 121102 (2013).
- [30] S. Wolgast, C. Kurdak, K. Sun, J. W. Allen, D.-J. Kim, and Z. Fisk, *Phys. Rev. B* **88**, 180405 (2013).
- [31] D. J. Kim, S. Thomas, T. Grant, J. Botimer, Z. Fisk, and J. Xia, *Sci. Rep.* **3**, 3150 (2013).
- [32] T. L. Anderson and H. B. Krause, *Acta Crystallogr. Sect. B* **30**, 1307 (1974).
- [33] M. Liu, J. Zhang, C.-Z. Chang, Z. Zhang, X. Feng, K. Li, K. He, L.-l. Wang, X. Chen, X. Dai, Z. Fang, Q.-K. Xue, X. Ma, and Y. Wang, *Phys. Rev. Lett.* **108**, 036805 (2012).
- [34] K. Nomura, M. Koshino, and S. Ryu, *Phys. Rev. Lett.* **99**, 146806 (2007).
- [35] S. Hikami, A. I. Larkin, and Y. Nagaoka, *Prog. Theor. Phys.* **63**, 707 (1980).
- [36] G. Bergmann, *Phys. Rep.* **107**, 1 (1984).
- [37] B. L. Altshuler, A. G. Aronov, and D. E. Khmel'nitsky, *J. Phys. C* **15**, 7367 (1982).
- [38] H.-T. He, G. Wang, T. Zhang, I.-K. Sou, G. K. L. Wong, J.-N. Wang, H.-Z. Lu, S.-Q. Shen, and F.-C. Zhang, *Phys. Rev. Lett.* **106**, 166805 (2011).
- [39] Y. S. Kim, M. Brahlek, N. Bansal, E. Edrey, G. A. Kapilevich, K. Iida, M. Tanimura, Y. Horibe, S.-W. Cheong, and S. Oh, *Phys. Rev. B* **84**, 073109 (2011).
- [40] M. Liu, C.-Z. Chang, Z. Zhang, Y. Zhang, W. Ruan, K. He, L.-l. Wang, X. Chen, J.-F. Jia, S.-C. Zhang, Q.-K. Xue, X. Ma, and Y. Wang, *Phys. Rev. B* **83**, 165440 (2011).
- [41] J. G. Checkelsky, Y. S. Hor, R. J. Cava, and N. P. Ong, *Phys. Rev. Lett.* **106**, 196801 (2011).
- [42] J. Chen, X. Y. He, K. H. Wu, Z. Q. Ji, L. Lu, J. R. Shi, J. H. Smet, and Y. Q. Li, *Phys. Rev. B* **83**, 241304 (2011).
- [43] H.-Z. Lu and S.-Q. Shen, *Phys. Rev. B* **84**, 125138 (2011).